Changes in the Arctic Ocean carbon cycle with diminishing ice cover

Michael D. DeGrandpre[1], Wiley Evans[2], Mary-Louise Timmermans[3], Richard A. Krishfield[4], William J Williams[5], and Michael Steele[6]

[1]University of Montana
[2]Hakai Institute
[3]Yale University
[4]Woods Hole Oceanographic Institution
[5]DFO-IOS, Sydney, BC
[6]University of Washington

November 22, 2022

Abstract

Less than three decades ago only a small fraction of the Arctic Ocean (AO) was ice free and then only for short periods. The ice cover kept sea surface COat levels lower relative to other ocean basins that have been exposed year round to ever increasing atmospheric levels. In this study, we evaluate sea surface COmeasurements collected over a 6-year period along a fixed cruise track in the Canada Basin. The measurements show that mean COlevels are significantly higher during low ice years. The COincrease is likely driven by ocean surface heating and uptake of atmospheric COwith large interannual variability in the contributions of these processes. These findings suggest that increased ice-free periods will further increase sea surface CO, reducing the Canada Basin's current role as a net sink of atmospheric CO.

Changes in the Arctic Ocean carbon cycle with diminishing ice cover

Michael DeGrandpre[1*], Wiley Evans[2], Mary-Louise Timmermans[3], Richard Krishfield[4], Bill Williams[5] and Michael Steele[6]

[1]University of Montana, Missoula, MT, USA.
[2]Hakai Institute, Heriot Bay, BC, Canada.
[3]Yale University, New Haven, CT, USA.
[4]Woods Hole Oceanographic Institution, Woods Hole, MA, USA.
[5]Institute of Ocean Sciences, Sidney, BC, Canada.
[6]University of Washington, Seattle, WA, USA.

Corresponding author: Michael DeGrandpre (michael.degrandpre@umontana.edu)

Abstract (150 words max)

Less than three decades ago only a small fraction of the Arctic Ocean (AO) was ice free and then only for short periods. The ice cover kept sea surface pCO_2 at levels lower relative to other ocean basins that have been exposed year round to ever increasing atmospheric levels. In this study, we evaluate sea surface pCO_2 measurements collected over a 6-year period along a fixed cruise track in the Canada Basin. The measurements show that mean pCO_2 levels are significantly higher during low ice years. The pCO_2 increase is likely driven by ocean surface heating and uptake of atmospheric CO_2 with large interannual variability in the contributions of these processes. These findings suggest that increased ice-free periods will further increase sea surface pCO_2, reducing the Canada Basin's current role as a net sink of atmospheric CO_2.

Plain Language Summary

The Arctic Ocean (AO) ice cover is decreasing, exposing the sea surface to exchange with the gases in the atmosphere. Consequently, anthropogenic CO_2 that has accumulated in the atmosphere can now more readily enter the AO. It is expected that this will lead to an increase in CO_2 in the AO but because of a lack of data in the region, a clear relationship has not been established. We have measured the partial pressure of CO_2 (pCO_2) in the Canada Basin of the AO during 5 cruises spanning 2012-2017. These data have revealed that the pCO_2 is higher during years when ice concentration is low, supporting the previous hypothesis. Using a model, we have shown that while uptake of atmospheric CO_2 has increased pCO_2, heating has also been important. These processes vary significantly from year to year, masking the likely increase in pCO_2 over time. Based on these results, we can expect that while the Canada Basin has been a sink for atmospheric CO_2, the uptake of atmospheric CO_2 will diminish in the coming years.

1. Introduction

The rapid loss of sea ice in the Arctic Ocean (AO) is well-documented (*Meier et al.*, 2014). Other changes in the AO are also becoming evident. Freshwater content is increasing due to sea ice melt and river runoff (e.g., *Yamamoto-Kawai et al.*, 2009; *Proshutinsky et al.*, 2009; *Krishfield et al.*, 2014). Sea surface temperature has also increased (e.g., *Steele et al.*, 2008; *Toole et al.*, 2010*; Perovich et al.*, 2011*; Timmermans*, 2015). This evolving physical environment is altering biological production (*Arrigo and van Dijken*, 2015; *Bergeron and Tremblay*, 2014) and food web structure (*Li et al.*, 2009; *Søreide et al.*, 2010; *Hunt et al.*, 2014). The carbon cycle in the AO is intimately connected to these processes (*Anderson and Macdonald*, 2015), but it is not clear how carbon sources and sinks are changing in the AO and if they could affect CO_2 accumulation in the atmosphere and sea surface.

Sea surface pCO_2 is a key carbon cycle parameter because it is used to determine air-sea CO_2 fluxes for global carbon budgets and for understanding the rate of ocean acidification. Despite this, sea surface pCO_2 measurements in the AO are spatially and temporally sparse. While pCO_2 measurements date back decades (*Kelley*, 1970) and have continued on sporadic research cruises

(*Bates et al.*, 2006; *Cai et al.*, 2010; *Jutterström and Anderson*, 2010; *Robbins et al.*, 2013; *Evans et al.*, 2015; *Ahmed et al.*, 2019), measurements are mostly from AO shelf regions in the summer and fall due to limited access to more heavily ice-covered regions. Few studies have included repeat shipboard pCO_2 measurements from the AO's deep basins. The interior basins comprise ~50% of the surface area of the AO (*Bates et al.*, 2011) and, because of their reduced seasonal variability compared to AO coastal margins, might provide an earlier indicator of changes in pCO_2 as the ice-free sea surface is exposed to present-day atmospheric CO_2 levels.

There is evidence from previous studies that pCO_2 levels in the oligotrophic AO basins are changing. *Cai et al.*, (2010), *Miller et al.*, (2014) and *Yasunaka et al.*, (2016; 2018) have found that pCO_2 has increased along the Chukchi shelf and slope and in the Canada Basin. While the AO is known to be a sink for atmospheric CO_2 (*Bates et al.*, 2011; *Arrigo et al.*, 2010; *Yasunaka et al.*, 2016, 2018; *Islam et al.*, 2016, 2017), its contribution to global air-sea CO_2 fluxes remains highly uncertain (*Anderson and Macdonald*, 2015). Estimated to uptake between 70 and 200 teragrams (Tg) carbon per year or 5 - 14% of the global uptake (*Bates et al.*, 2011; *Yasunaka et al.*, 2018), continued ice loss will make these estimates even more uncertain. Increased CO_2 uptake by the AO will also accelerate ocean acidification, i.e, driving a commensurate decrease in pH that increases calcium carbonate solubility (*Yamamoto-Kawai et al.*, 2009; *Robbins et al.*, 2013). In this manuscript, a shipboard pCO_2 time-series collected from 2012-2017 in the AO's Canada Basin reveals that pCO_2 increases with decreasing ice concentration. We use a temporal reference, days since ice retreat (DSR), and a mass balance model to examine to what extent ice-dependent processes such as air-sea CO_2 fluxes, surface ocean warming and biological production drive changes in sea surface pCO_2 after ice retreats.

2. Methods

Observations. Underway sea surface pCO_2 was measured on the Beaufort Gyre Observing System/Joint Ocean Ice Study (BGOS/JOIS) cruises on the CCGS Louis S. St-Laurent during 2012-2017. No pCO_2 measurements were made in 2015. The starting dates for the five ~4 week cruises were Aug. 6, 2012, Aug. 3, 2013, Sept. 25, 2014, Sept. 24, 2016 and Sept. 8, 2017. The pCO_2 was recorded using an infrared-gas equilibrator system (SUPER-CO_2, Sunburst Sensors, LLC) located in the ship's lab. The instrument uses an infrared analyzer (LI-COR, LI-840A) and gas

phase equilibrator (Liqui-Cel membrane contactor, Model #G453) as described in *Hales et al.*, (2003). The equilibrator was connected directly to the ship's seawater line. Calibrations were automated using CO_2 gas standards and a zero CO_2 gas sample. Temperature was measured in the equilibrator and at the seawater intake (9 m depth), assumed equal to sea surface temperature (SST), as discussed below. The infrared analyzer CO_2 mole fraction was corrected to SST and converted to pCO_2 using 100% humidity at SST and local barometric pressure (*Dickson et al.*, 2007). Some warming, usually <0.5 °C, can occur enroute to the equilibrator so it is essential to correct the pCO_2 for this temperature change. If there were greater than ~2°C differences between the equilibrator inlet temperature and SST, it was assumed seawater flow had stopped (e.g., due to ice clogging) and the pCO_2 was discarded during these periods. A flow meter was installed in 2016 to detect periods of low flow rate. The pCO_2 uncertainty is estimated to be ±5 µatm based on the reproducibility of the standards and baseline zero. CTD stations showed that the seawater intake was sometimes within the halocline (i.e., below the mixed layer) and this was also evident from the salinity and temperature variability recorded by the ship's thermosalinograph. These conditions were found mostly on the continental shelf during 2012 and 2013 due to high Mackenzie River outflow. This analysis focuses on the Canada Basin bounded by 155-130° W and 72-82° N where CTD stations consistently found that mixed layer depths were greater than the ship intake depth.

Air temperature, wind speed (25 m height), wind direction, and barometric pressure were recorded by the ship's weather system. Mixed layer depths, defined as the depth where the density difference from the surface first exceeds 0.25 kg m^{-3} (*Timmermans, et al.,* 2012), were determined using temperature and salinity from ~50 CTD casts occupied annually as part of the BGOS/JOIS cruises (Proshutinsky et al. 2019). Atmospheric pCO_2 was computed from the mole fraction of CO_2 measured at Alert, Nunavut, Canada using data from the National Oceanic and Atmospheric Administration (NOAA) Earth System Research Laboratory (ESRL) (https://www.esrl.noaa.gov). Sea ice concentration with daily, 12 km resolution was obtained from the French Research Institute for Exploration of the Sea (IFREMER) (http://cersat.ifremer.fr/oceanography-fromspace/our-domains-of-research/sea-ice) that provides data collected by the satellite-based Special Sensor Microwave Imager (SSM/I) and processed by the National Snow and Ice Data Center (https://nsidc.org).

Data analysis and modeling. In this study our goals are to determine if sea surface pCO_2 levels are related to interannual variability in ice concentration and to evaluate processes that might control pCO_2 under low ice conditions. To facilitate analysis of the spatially and temporally disparate shipboard pCO_2 and other data, Canada Basin data were gridded by identifying 20x20 km grid areas that contain data, and those data were then averaged as described in *Evans et al.* (2015). The gridding routine computed the average and standard deviation of data found within each grid cell as well as the number of observations. The average number of observations for each grid cell ranged from 17-23 over the 5 cruises. The gridded data were spatially averaged for each cruise (i.e. each year) to allow interannual comparisons of the physical and biogeochemical conditions. Further, we used these yearly values as input to the mass balance model described below.

The mass balance model was used to examine how sea surface pCO_2 might change after ice retreats. Many processes contribute to sea surface pCO_2 variability including biological production, heating and cooling, physical mixing and upwelling, ice melt and formation and air-sea gas exchange. Sea surface warming and air-sea uptake are likely the most important factors for increasing pCO_2 in low ice areas in the Canada Basin (*Cai et al.*, 2010; *Else et al.*, 2013). The combined contributions of these two processes to sea surface pCO_2 variability were estimated using a dissolved inorganic carbon (DIC) mixed-layer mass balance (*Martz et al.*, 2009; *Islam et al.*, 2017) as follows,

$$\Delta DIC = F_{gasex} \times \Delta t/(MLD \times \rho) \quad (1)$$

where ΔDIC is the change in DIC for a time step Δt (1 hr in this study), F_{gasex} is the air-sea CO_2 flux (e.g., in mmol m^{-2} d^{-1}), MLD is the mixed-layer depth, and ρ is seawater density. Warming (increasing SST) is accounted for in the equilibrium calculation as described below. F_{gasex} was calculated using

$$F_{gasex} = k \times K_0 \times \Delta pCO_2 \times f, \quad (2)$$

where k is the gas transfer velocity, K_0 is the CO_2 solubility, ΔpCO_2 is the pCO_2 difference be-

tween the sea surface and atmosphere, and f is the fraction of open water (*Prytherch et al.*, 2017; *Butterworth and Miller*, 2016). In this case, f is set equal to 1 because the pCO_2 was modeled only after the day of ice retreat (DOR), i.e. when ice concentration dropped below 15% in any grid cell (*Steele and Dickinson*, 2016), a value that is within the uncertainty of the satellite data (*Ivanova et al.*, 2015). F_{gasex} is negative when there is a net uptake of CO_2 by the ocean from the atmosphere. We used the wind speed relationship in *Wanninkhof* (2014) to compute k, where ship wind speed was corrected to 10 m height. The average of second moments of wind speed (i.e., wind speed^2) were calculated as opposed to wind speed averages because short-term (< daily) variability in the winds is retained leading to higher gas transfer rates during periods of greater wind speed variability (*Wanninkhof*, 2014; *Evans et al.*, 2015).

To examine potential contributions from biological production, net community production (NCP) was added to the mass balance,

$$\Delta DIC = (F_{gasex} + F_{NCP}) \times \Delta t/(MLD \times \rho) \quad (3)$$

where F_{NCP} is the net uptake of CO_2 due to biological production (e.g. in mmol m^{-2} d^{-1}). We used values from *Ji et al.* (2019) who measured NCP using O_2 isotope and O_2/argon methods during the same BGOS cruises, excluding 2017. In the mass balance models (i.e., Equations 1 and 3), DIC was incremented for each time step with ΔDIC from Equation 1 or Equation 3. The pCO_2 was then recalculated using the new DIC, SST and salinity and a constant total alkalinity (A_T) in the equilibrium program CO2sys (*Pierrot et al.*, 2006). The A_T was estimated using an A_T-salinity relationship derived from bottle samples during the BGOS cruises (*Yamamoto-Kawai et al.*, 2005; *DeGrandpre et al.*, 2019). A_T is a conservative property of seawater that does not change with temperature or air-sea CO_2 exchange (*Millero*, 2007). The duration of the model calculation is based on the maximum number of days since ice retreat (DSR) computed as the difference between the mean pCO_2 measurement date and the mean day of ice retreat (DOR) for all pCO_2 observations in each grid cell. For surface warming, SST was incremented equally for each time step from -1.5°C to the mean SST (Table 1) from DSR = 0 days until the end of the DSR period similar to *Else et al.*, (2013). The initial under-ice condition was chosen to be the freezing point of seawater at a salinity of 27 (-1.5° C) and a seawater pCO_2 of 300 µatm all derived from extrapolation of the mean gridded data versus mean ice concentration to 100% ice

concentration. All equilibrium (CO2sys) calculations used the *Mehrbach et al.* (1973) constants refit by *Dickson and Millero* (1987). Lastly, mean gridded values were used in the model calculations (Table 1, Equations 1-3). A model that uses the evolution of ice concentration at each grid cell and includes other changing physical conditions, e.g. MLD or wind, was beyond the scope of this study.

Table 1: Mean cruise values used in the mass balance model derived from ship measurements and other sources (see Methods).							
Year	Mean pCO_2 (µatm)	Sea ice concen-tration (%)	Wind speed ($m\ s^{-1}$)	Atm. pCO_2 (µatm)	SST (°C)	Salinity	Mixed lay-er depth (m)
2012	365 ± 34	8 ± 22	8.1 ± 1.1	379 ± 3	2.5 ± 3.6	25.5 ± 1.4	12.1 ± 6.6
2013	327 ± 24	59 ± 38	5.0 ± 1.0	384 ± 3	-0.1 ± 1.6	26.7 ± 0.8	15.5 ± 5.5
2014	318 ± 14	78 ± 32	5.8 ± 0.7	392 ± 4	0.6 ± 2.2	27.0 ± 0.7	27.2 ± 4.3
2016	371 ± 23	21 ± 37	6.6 ± 0.3	395 ± 3	-0.3 ± 1.0	27.1 ± 0.7	26.1 ± 4.7
2017	350 ± 21	19 ± 33	7.3 ± 0.7	395 ± 2	1.1 ± 1.9	26.9 ± 1.0	26.5 ± 5.1

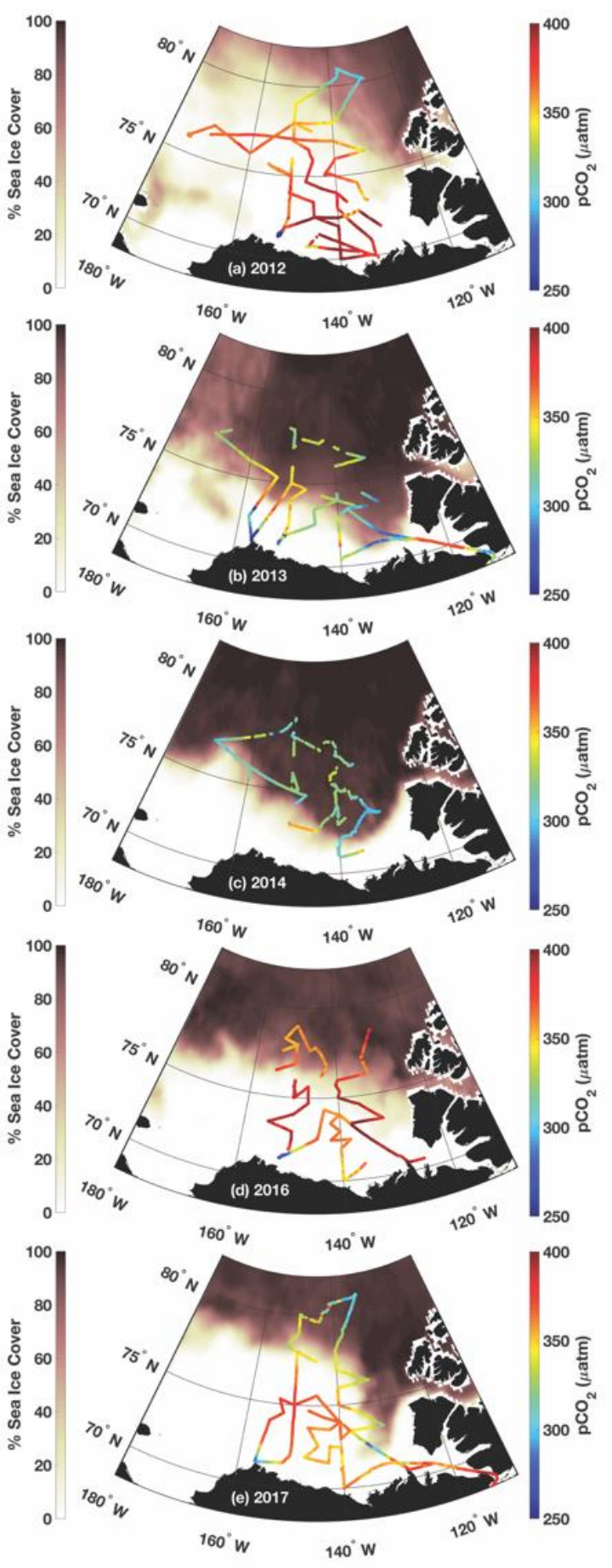

Figure 1: Sea surface partial pressure of CO_2 (pCO_2) data obtained on the Canadian icebreaker CCGS Louis S. St-Laurent from 2012-2017. The pCO_2 levels are indicated by the color along the ship cruise track (right color bar). The dark shaded coloration (left color bar) represents sea ice concentration averaged from the daily satellite data collected over the course of each cruise. Data for this analysis were taken from the area bracketed by 155-130° W, 72-82° N in the Canada Basin. The ship visited the same stations each year but the cruise track varied to support other field studies and various other activities. The data gaps in 2013 were due to problems with the seawater intake. The starting dates for the five ~4 week cruises were Aug. 6, 2012, Aug. 3, 2013, Sept. 25, 2014, Sept. 24, 2016 and Sept. 8, 2017, top to bottom, respectively. No pCO_2 measurements were made in 2015.

190

3. Results and Discussion

The shipboard pCO_2 data collected on the Beaufort Shelf, Canada Basin, and eastern Chukchi Sea are shown in Figure 1 overlaid on % sea ice concentration. A large range of interannual variability in sea ice cover was observed during these cruises. In 2012, ice cover dropped to 3.4 million km^2, the lowest level observed since the satellite record began in 1978. The minimum ice extent rebounded in 2013 and 2014 to ~5.0 million km^2. All five years ranked in the top 10 lowest minima (National Snow and Ice Data Center, Arctic Sea Ice News and Analysis, http://nsidc.org/arcticseaicenews). Sea surface pCO_2 was also highly variable spatially and interannually. Open water in the Canada Basin typically had higher pCO_2 levels than pCO_2 recorded in ice-covered areas; for example, compare 2012 (low ice) and 2014 (more ice) in Figure 1.

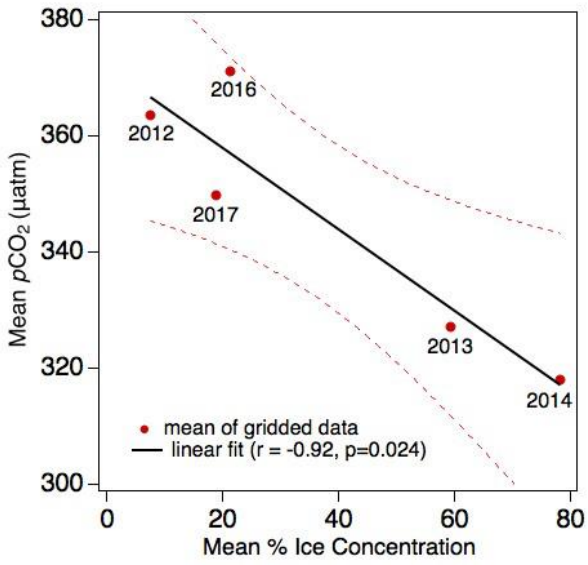

Figure 2: Canada Basin mean pCO_2 vs. mean sea ice concentration for each cruise shown in Figure 1. Symbols are labeled with each year. Means were computed using data gridded to a 20x20 km area in the region spanning 155-130° W and 72-82° N. The 95% confidence bands are included (dashed red curves). No measurements were made in 2015.

Using the mean pCO_2 levels for each cruise reveals a significant correlation with ice concentration (Figure 2). Sea surface pCO_2 is higher and closer to atmospheric saturation during years of low ice concentration and exceeded atmospheric pCO_2 (Table 1) in some locations in 2012 and 2016 (Figure 1). Although sparser data sets over different regions have found evidence that sea surface pCO_2 in the AO is increasing with decreasing ice cover (*Cai et al.*, 2010; *Jutterström and*

Anderson, 2010; *Else et al.*, 2013), no previous studies have documented a clear connection like that shown in Figure 2. The mean pCO_2 values from each cruise reveal this relationship with ice concentration by consolidating the variability – the gridded pCO_2 for each cruise covers the full range shown in Figure 2 obscuring interannual differences (Figure 1S).

The absence of sea ice exposes the surface ocean to direct solar radiation and atmospheric heating and the subsequent warming increases pCO_2. Air-sea exchange will also increase sea surface pCO_2 because, when the pCO_2 is lower than atmospheric levels, the AO will absorb CO_2 from the atmosphere (Figure 1, Table 1). These mechanisms for increasing pCO_2 in the surface ocean infer that pCO_2 is not only dependent upon the ice cover but also the duration of open water (*Arrigo and van Dijken*, 2015). Thus, the days since ice retreat (DSR) is used as a temporal reference, as defined above. We examine specific variables that might be important in driving the relationship between pCO_2 and sea ice concentration, including DSR, sea-surface temperature (SST), MLD, wind speed and NCP (Equations 1-3, Table 1).

The gridded sea surface pCO_2 shows mostly increasing values after ice retreat with large intra and interannual variability (Figure 3). Each year's observations appear to have a relatively consistent upward trajectory, except for 2016 and 2017 (discussed below), suggesting similar processes were at work in the open water area of the Canada Basin during each cruise. The pCO_2 observations have more scatter with increasing DSR, possibly due to different physical conditions during each cruise and each year. Some of the interannual variability may be due to differences in cruise timing, but there are significant contrasts between cruises conducted over similar periods. For example, in Figure 2, the mean pCO_2 from the August cruises (2012 and 2013) differ significantly, as do data from the late September cruises (2014 and 2017). These differences are also evident in the pCO_2 data in Figure 3 with lower values in 2013 and 2014 compared to 2012 and 2016, respectively.

The results of the mass balance model are also shown in Figure 3. The model encompasses the range of observed variability using the mean conditions in Table 1. Although there is disagreement between observations and model curves during some years and some parts of the records, these results suggest that heating and/or gas exchange significantly contribute to the observed

increase in pCO_2 with increasing DSR and that these processes are highly variable from year to year (broken down in Figure 3S). In 2012, the model predicts that heating and gas exchange increased pCO_2 by ~60 and ~30 µatm, respectively; whereas in 2016, heating and gas exchange contributions were ~15 and ~65 µatm, respectively (Figure 3S). Also note that a smaller range of variability is observed and predicted for the cruise data with shorter DSR periods (2013 and 2014) (Figure 3 and Figure 3S), where surface ocean warming and air-sea gas exchange were limited by the time of exposure to the atmosphere.

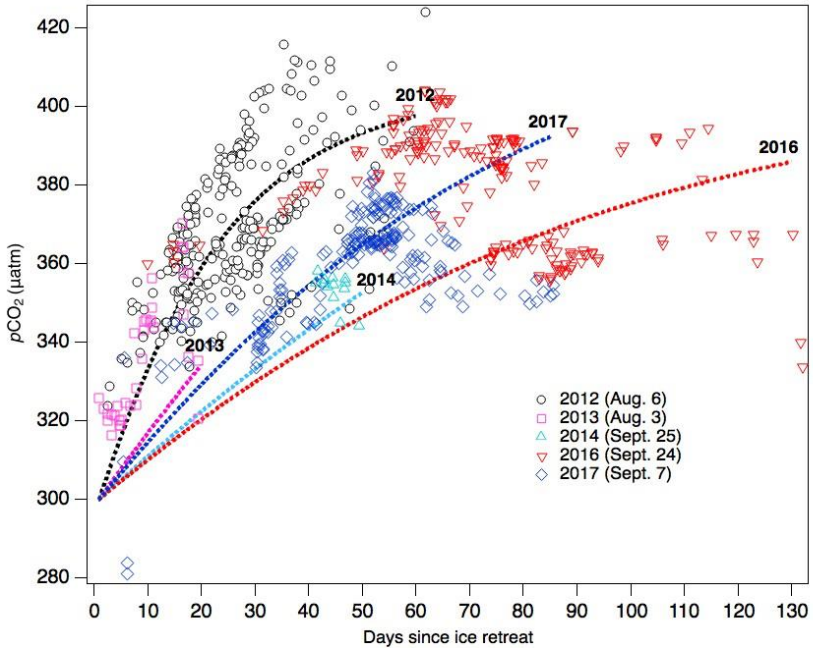

Figure 3: Gridded pCO_2 observations (symbols) vs. days since ice retreat (DSR) from 2012-2017, excluding 2015. Modeled pCO_2 (dashed curves, labeled with each year and with the color matching the pCO_2 symbol data) were computed from the predicted change in pCO_2 due to air-sea exchange and increase in SST using values in Table 1. Models were run to the maximum DSR recorded for each cruise period. Initial pCO_2 before loss of ice was assumed to be 300 µatm (see Methods). The cruise start dates are indicated in parentheses in the legend.

There are other possible sources of variability and incorrect model assumptions that could contribute to differences between the model and observations. The sensitivity analysis in the Supplemental Information (SI) shows that much (but not all) of the variability within each cruise can be explained by varying input values over the observed ranges (Figure 2S, Table 1). There are

some other notable deviations, however. For example, during 2016 and 2017, the two years with extended DSRs, the pCO_2 levels decreased after ~60 days (Figure 3). In these years, data were collected into October, at which point sea surface cooling is possible which would decrease the pCO_2. Because the model employs a linear warming trend, it can only predict the mean change not the time-varying rate of warming or cooling. We did not manipulate the rate of heating or introduce an arbitrary period of cooling because this would essentially be fitting to the data. However, the hypothesis that surface cooling drove the observed decreases in pCO_2 for these years is a plausible scenario. It is important to note that movement of the ship into different water masses over the course of each cruise may have also contributed to the scatter. For example, the drop in pCO_2 after 60 days in 2017 corresponds to a period of lower salinity (not shown). Also, employing DSR as a time variable in the model assumes that no air-sea exchange or warming occurred when sea ice concentration was greater than 15% which is clearly not true (Figure 1S). While we could not readily model gas exchange prior to DOR in this study, the heating contribution was likely small because no SST data exceeded 0.0 °C from 0 to 10 days after ice retreat. An increase of from -1.5°C, the approximate freezing point, to 0.0°C would increase pCO_2 by ~22 µatm. *Steele and Dickinson* (2016) also found that SST is typically < 0°C at DOR. Ice melt and formation could change pCO_2 by diluting and concentrating DIC, respectively, and by altering the ratio of DIC and A_T in the ice or brine (*Rysgaard et al.,* 2007, 2009; *Cai et al.,* 2010; *DeGrandpre et al.*, 2019). Ice melt occurs before DOR and could decrease pCO_2 levels (*Cai et al.,* 2010). In fact, heating, gas exchange and ice melt may have all played a role in determining the pre-DOR pCO_2 levels, contributing to the deviations between model and observations evident in Figure 3.

Lastly, we consider possible biological contributions to the observed variability. Biological drawdown of sea surface pCO_2 in the Canada Basin is predicted to be small because of the lack of nutrients in the stratified surface layer. The study by *Cai et al.* (2010) found no evidence of a biological DIC drawdown in the Canada Basin for waters > 72°N. In a previous study in the Canada Basin, an NCP ~4.9 mmol O_2 $m^{-2}d^{-1}$ offset a ~15 µatm pCO_2 increase expected from atmospheric CO_2 uptake in low ice conditions (*Islam et al.*, 2017). The *Ji et al.* (2019) NCP values, which ranged from 1.3 to 2.9 mmol O_2 $m^{-2}d^{-1}$ from 2011-2016, confirm the very low productivity for the Canada Basin (Bates et al. 2005). For comparison, in the same paper, NCP in the eastern

Chukchi Sea was estimated to range from 30 to 240 mmol $m^{-2}d^{-1}$. The Canada Basin rates have a relatively small effect on the modeled pCO_2 levels, estimated using Equation 3. In 2012, the pCO_2 would be reduced by 8-25 µatm by the end of the DSR period (60 days) over the range of NCP reported in *Ji et al.* (2019) (Figure 2S). These estimates assume the rate of NCP was constant over the DSR period. The O_2/argon method integrates NCP over the residence time of O_2 in the mixed layer (10-30 days) (*Kaiser et al.*, 2005) and the rates in *Ji et al.* (2019) varied by only 15-21% during the cruises. This range of variability would not significantly alter the modeled pCO_2 trajectory (Figure 2S, Table 1S).

4. Conclusions

This study reveals that loss of sea ice leads to increased sea surface pCO_2 levels in the Canada Basin. Using the DSR as a temporal reference facilitated implementation of a time-dependent mass balance model to explore the underlying mechanisms that might control sea surface pCO_2 in open water conditions. Results from the model suggest that warming and air-sea uptake drive the pCO_2 towards atmospheric equilibrium to a varying extent (Figure 3 and Figure 3S). NCP is persistently low and can only account for a small portion of the observed interannual variability (Figure 2S, Table 1S). These results suggest that neither of two previously proposed scenarios, i.e. that increased SST will largely negate uptake of atmospheric CO_2 (*Else et al.*, 2013) or that air-sea gas exchange will consistently dominate the increase in pCO_2 (*Cai et al.*, 2010; *Bates et al.*, 2006) (Figure 2S). An important implication, as discussed by others (*Cai et al.*, 2010), is that increased SSTs can reduce the uptake of atmospheric CO_2 by increasing the rate at which pCO_2 rises towards atmospheric equilibrium, decreasing the air-sea CO_2 gradient. The model prediction suggests that warming reduced the possible air-sea CO_2 flux by 55% in 2012, the year with the most warming (Figure 3S). As Arctic warming and open water periods increase, it is possible that, as observed in 2012, the lowest ice concentration year on record, pCO_2 will more frequently exceed atmospheric saturation. These results also imply that CO_2 is accumulating from year to year in the Canada Basin. Even with the insights provided in this study, the future response of the AO carbon cycle to decreased seasonal ice cover remains highly uncertain and can only be understood by continued observations and modeling.

Acknowledgments

Cory Beatty (University of Montana) operated the underway pCO_2 system. Fakhrul Islam and Brittany Peterson (University of Montana) helped with data analysis. Sarah Zimmerman (Institute of Ocean Sciences) facilitated installation of the pCO_2 system and oversaw the seawater line measurements. The underway pCO_2 instrument (SUPER-CO_2) and technical support were provided by Sunburst Sensors. We thank Andrey Proshutinsky (WHOI) for his leadership as co-PI of the BGOS program. Additional vital logistical support was provided by WHOI personnel. The reviewers' comments significantly improved the manuscript. The data are available through the U.S. National Science Foundation (NSF) Arctic Data Center (https://arcticdata.io) (doi:10.18739/A2R785P3X). This research was made possible by grants from the NSF Arctic Observing Network program (ARC-1107346, PLR-1302884, PLR-1504410 and OPP-1723308). In addition, M.S. was supported by ONR grant 00014-17-1-2545, NASA grant NNX16AK43G, and NSF grants PLR-1503298 and OPP-1751363.

References

Ahmed, M., Else, B. G. T., Burgers, T. M., and T. Papakyriakou (2019), Variability of surface water pCO_2 in the Canadian Arctic Archipelago from 2010 to 2016. *J. Geophys. Res. Oceans*, 124, 1876–1896.

Anderson, L. G., and R. W. Macdonald (2015), Observing the Arctic Ocean carbon cycle in a changing environment, *Polar Research*, 34, 26891, http://dx.doi.org/10.3402/polar.v34.26891.

Arrigo, K. R. and G. L. van Dijken (2015), Continued increases in Arctic Ocean primary production, *Prog. Oceanogr.*, 136, 60-70, doi:10.1016/j.pocean.2015.05.002.

Arrigo, K. R., S. Pabi, G. L. van Dijken, and W. Maslowski (2010), Air-sea flux of CO_2 in the Arctic Ocean, 1998–2003, *J. Geophys. Res.*, 115, G04024, doi:10.1029/2009JG001224.

Bates, N.R., W.-J. Cai, and J.T. Mathis (2011), The ocean carbon cycle in the western Arctic Ocean: Distributions and air-sea fluxes of carbon dioxide. *Oceanography* 24, 186–201, http://dx.doi.org/10.5670/oceanog.2011.71.

Bates, N. R., S. B. Moran, D. A. Hansell, and J. T. Mathis (2006), An increasing CO_2 sink in the Arctic Ocean due to sea-ice loss, *Geophys. Res. Lett.*, 33, L23609,

doi:10.1029/2006GL027028.

Bates, N. R., M. H. P. Best, and D. A. Hansell (2005), Spatio-temporal distribution of dissolved inorganic carbon and net community production in the Chukchi and Beaufort Seas, *Deep Sea Research Part II: Topical Studies in Oceanography*, 52, 3303-3323.

Bergeron, M., and J.-É. Tremblay (2014), Shifts in biological productivity inferred from nutrient drawdown in the southern Beaufort Sea (2003–2011) and northern Baffin Bay (1997–2011), Canadian Arctic, *Geophys. Res. Lett.*, 41, 3979–3987, doi:10.1002/2014GL059649.

Butterworth, B. J., and S. D. Miller (2016), Air-sea exchange of carbon dioxide in the Southern Ocean and Antarctic marginal ice zone, *Geophys. Res. Lett.*, 43, 7223–7230, doi:10.1002/2016GL069581.

Cai W., *et al.* (2010), Decrease in the CO_2 uptake capacity in an ice-free Arctic Ocean basin, *Science*, 329, 556, doi: 10.1126/science.1189338.

DeGrandpre, M.D., C-Z. Lai, M.-L. Timmermans, R. A. Krishfield, A. Proshutinsky, and D. Torres (2019), Inorganic carbon and pCO_2 variability during ice formation in the Beaufort Gyre of the Canada Basin, *Journal of Geophysical Research – Oceans,* 124, https://doi.org/10.1029/2019JC015109.

Dickson, A.G., C. L. Sabine, and J. R. Christian (Eds.) (2007), Guide to best practices for ocean CO_2 measurements, PICES Special Publication, 3, 191 pp.

Dickson, A., and F. Millero (1987), A comparison of the equilibrium constants for the dissociation of carbonic acid in seawater media, *Deep Sea Res., Part A*, 34, 1733–1743, doi:10.1016/0198-0149(87)90021-5.

Else G.T., R. J. Galley, B. Lansard, D. G. Barber, K. Brown, L. A. Miller, A. Mucci, T. N. Papakyriakou, J.-É. Tremblay, and S. Rysgaard (2013), Further observations of a decreasing atmospheric CO_2 uptake capacity in the Canada Basin (Arctic Ocean) due to sea ice loss, *Geophys. Res. Lett.*, 40, 1132-1137, doi:10.1002/grl.50268.

Evans, W., J. T. Mathis, J. N. Cross, N. R. Bates, K. E. Frey, B. G. T. Else, T. N. Papkyriakou, M. D. DeGrandpre, F. Islam, W.-J. Cai, B. Chen, M. Yamamoto-Kawai, L. A. Miller, E. Carmack, W. J. Williams, and T. Takahashi (2015), Sea-air CO_2 exchange in the western Arctic coastal ocean, *Global Biogeochem. Cycles*, 10.1002/2015GB005153.

Hales, B., D. W. Chipman, and T. Takahashi (2004), High frequency measurement of partial pressure and total concentration of carbon dioxide in seawater using microporous hydrophobic membrane contactors, *Limnol. Oceanog: Methods*, *2*, 356-364.

Hunt, B. P. V., R. J. Nelson, B. Williams, F. A. McLaughlin, K. Young, K. A. Brown, S. Vagle, and E. C. Carmack (2014), Zooplankton community structure and dynamics in the Arctic Canada Basin during a period of intense environmental change (2004–2009), *J. Geophys. Res. Oceans*, 119, 2518–2538, doi:10.1002/2013JC009156.

Islam, F., M. DeGrandpre, C. Beatty, R. Krishfield, and J. Toole (2016), Gas exchange of CO_2 and O_2 in partially ice-covered regions of the Arctic Ocean investigated using in situ sensors, *IOP Conf. Series: Earth and Environmental Science*, 35, doi:10.1088/1755-1315/35/1/012018.

Islam, F., DeGrandpre, M., Beatty, C., Timmermans, M.-L., Krishfield, R., Toole, J. and S. Laney (2017), Sea surface pCO_2 and O_2 dynamics in the partially ice-covered Arctic Ocean, *J. Geophys. Res. – Oceans*, 122, doi:10.1002/2016JC012162.

Ivanova, N. et al (2015), Inter-comparison and evaluation of sea ice algorithms: towards further identification of challenges and optimal approach using passive microwave observations, *The Cryosphere*, 9, 1797–1817.

Ji, B.Y., Sandwith, Z. O., Williams, W. J., Diaconescu, O., Ji, R., Li, Y., Van Scoy, E., Yamamoto-Kawai, M., Zimmermann, S. and R. H. R. Stanley (2019), Variations in rates of biological production in the Beaufort Gyre as the Arctic changes: Rates from 2011 to 2016, *J. Geophys. Res. – Oceans*, doi.org/10.1029/2018JC014805.

Jutterström, S. and L. G. Anderson (2010), Uptake of CO_2 by the Arctic Ocean in a changing climate, *Mar. Chem.*, 122, 96–104.

Kaiser, J., M. K. Reuer, B. Barnett, and M. L. Bender (2005), Marine productivity estimates from continuous O_2/Ar ratio measurements by membrane inlet mass spectrometry, *Geophys. Res. Lett.*, 32, L19605, doi:10.1029/2005GL023459.

Kelley Jr., J. J. (1970), Carbon dioxide in the surface waters of the North Atlantic and the Barents and Kara Sea, *Limnol. Oceanogr.*, 15, 80–87.

Krishfield, R. A., A. Proshutinsky, K. Tateyama, W. J. Williams, E. C. Carmack, F. A. McLaughlin, and M.-L. Timmermans (2014), Deterioration of perennial sea ice in the Beaufort Gyre from 2003 to 2012 and its impact on the oceanic freshwater cycle, *J. Geophys. Res.*, 119, doi:10.1002/2013JC008999.

Li, W. K., F. A. McLaughlin, C. Lovejoy, and E. C. Carmack (2009), Smallest algae thrive as the Arctic Ocean freshens, *Science*, 326, 539–539, doi:10.1126/science.1179798.

Martz, T.M., DeGrandpre, M.D., Strutton, P.G., McGillis, W.R. and W. Drennan (2009), Sea surface pCO_2 and carbon export during the Labrador Sea spring-summer bloom: an in situ mass balance approach, *J. Geophys. Res. - Oceans*, 114, C09008, doi:10.1029/2008JC005060.

Mehrbach, C., C. H. Culberson, J. E. Hawley, and R. M. Pytkowicz (1973), Measurement of the apparent dissociation constants of carbonic acid in seawater at atmospheric pressure, *Limnology and Oceanography*, 18, 897–907.

Meier, W. N., et al. (2014), Arctic sea ice in transformation: A review of recent observed changes and impacts on biology and human activity, *Rev. Geophys.*, 51,185–217, doi:10.1002/2013RG000431.

Miller, L.A., R.W. Macdonald, A. Mucci, M. Yamamoto-Kawai, K.E. Giesbrecht, F. McLaughlin, and W.J. Williams (2014), Changes in the marine carbonate system of the western Arctic: Patterns in a rescued data set. *Polar Res*., 33, 20577, doi: 10.3402/polar.v33.20577.

Millero, F.J. (2007), The marine inorganic carbon cycle, *Chem. Rev*., 107, 308-341.

Perovich, D., K. Jones, B. Light, H. Eicken, T. Markus, J. Stroeve, and R. Lindsay (2011), Solar partitioning in a changing Arctic sea-ice cover, *Ann. Glaciol.*, 52(57), 192–196.

Pierrot, D., Lewis, E. and D.W.R. Wallace (2006), MS Excel program developed for CO_2 system calculations. ORLN/CDIAC-105, Carbon Dioxide Information Analysis Center, Oak Ridge National Laboratory, U.S. Department of Energy, Oak Ridge, Tennessee.

Proshutinsky, A., R. Krishfield, M.-L. Timmermans, J. Toole, E. Carmack, F. McLaughlin, W. J. Williams, S. Zimmermann, M. Itoh, and K. Shimada (2009), Beaufort Gyre freshwater reservoir: State and variability from observations, *J. Geophys. Res.*, 114, C00A10, doi:10.1029/2008JC005104.

Proshutinsky, A., R. Krishfield and M.-L. Timmermans (2019), Preface to special issue Forum for Arctic Ocean Modeling and Observational Synthesis (FAMOS) 2: Beaufort Gyre phenomenon, *J. Geophys. Res.-Oceans*, https://doi.org/10.1029/2019JC015400.

Prytherch, J., I. M. Brooks, P. M. Crill, B. F. Thornton, D. J. Salisbury, M. Tjernström, L. G. Anderson, M. C. Geibel, and C. Humborg (2017), Direct determination of the air-sea CO_2 gas transfer velocity in Arctic sea ice regions, *Geophys. Res. Lett.*, 44,3770–3778.

Robbins, L.L., J. G. Wynn , J. T. Lisle, K. K. Yates, P. O. Knorr, R. H. Byrne, X. Liu, M. C. Patsavas, K. Azetsu-Scott, and T. Takahashi (2013), Baseline monitoring of the western Arctic Ocean estimates 20% of Canadian Basin surface waters are undersaturated with respect to aragonite, *PLoS ONE*, 8, e73796, doi:10.1371/journal.pone.0073796.

Rysgaard, S., R. N. Glud, M. K. Sejr, J. Bendtsen, and P. B. Christensen (2007), Inorganic carbon transport during sea ice growth and decay: A carbon pump in polar seas, *J. Geophys. Res.*, 112, C03016, doi: 10.1029/2006JC003572.

Rysgaard, S., J. Bendtsen, L. T. Pedersen, H. Ramløv, and R. N. Glud (2009), Increased CO2 uptake due to sea ice growth and decay in the Nordic Seas, *J. Geophys. Res.*, 114, C09011, doi:10.1029/2008JC005088.

Søreide, J. E., E. V. A. Leu, J. Berge, M. Graeve, and S. Falk-Petersen (2010), Timing of blooms, algal food quality and Calanus glacialis reproduction and growth in a changing Arctic, *Global Change Biol.*, 16**,** 3154-3163.

Steele, M., and S. Dickinson (2016), The phenology of Arctic Ocean surface warming, *J. Geophys. Res. Oceans*, 121, 6847–6861, doi:10.1002/2016JC012089.

Steele, M., W. Ermold, and J. Zhang (2008), Arctic Ocean surface warming trends over the past 100 years, *Geophys. Res. Lett.*, 35, L02614, doi:10.1029/2007GL031651.

Timmermans, M.-L. (2015), The impact of stored solar heat on Arctic sea-ice growth. *Geophys. Res. Lett.*, 42, doi:10.1002/2015GL064541.

Timmermans, M.-L., S. Cole, and J. Toole (2012), Horizontal density structure and restratification of the Arctic Ocean surface layer, *J. Phys. Oceanogr.*, 42, 659–668, doi.org/10.1175/JPO-D-11-0125.1.

Toole, J. M., M.-L. Timmermans, D. K. Perovich, R. A. Krishfield, A. Proshutinsky, and J. A. Richter-Menge (2010), Influences of the ocean surface mixed layer and thermohaline stratification on Arctic Sea ice in the central Canada Basin, *J. Geophys. Res.*, 115 , C10018, doi:10.1029/2009JC005660.

Wanninkhof, R. (2014), Relationship between wind speed and gas exchange over the ocean revisited, *Limnol. Oceanogr.: Methods*, 12, 351–362, doi: 10.4319/lom.2014.12.351.

Yamamoto-Kawai, M., N. Tanaka, and S. Pivovarov (2005), Freshwater and brine behaviors in the Arctic Ocean deduced from historical data of $\delta^{18}O$ and alkalinity (1929-2002 A.D.), *J. Geophys. Res.*, 110, C10003, doi: 10.1029/2004JC 002793.

Yamamoto-Kawai, M., F. A. McLaughlin, E. C. Carmack, S. Nishino, and K. Shimada (2009), Aragonite undersaturation in the Arctic Ocean: Effects of ocean acidification and sea ice melt, *Science*, 326, 1098-1100, doi: 10.1126/science. 1174190.

Yasunaka, S., A. Murata, E. Watanabe, M. Chierici, A. Fransson, S. van Heuven, M. Hoppema, M. Ishii, T. Johannessen, N. Kosugi, S. K. Lauvset, J. T. Mathis, S. Nishino, A. M. Omar, A. Olsen, D. Sasano, T. Takahashi and R. Wanninkhof (2016), Mapping of the air–sea CO_2 flux in the Arctic Ocean and its adjacent seas: basin-wide distribution and seasonal to interannual variability, *Polar Science*, 10, 323–334, doi:10.1016/j.polar.2016.03.006.

Yasunaka, S., E. Siswanto, A. Olsen, M. Hoppema, E. Watanabe, A. Fransson, M. Chierici, A. Murata, S. K. Lauvset, R. Wanninkhof, T. Takahashi, N. Kosugi, A. M. Omar, S. van Heuven and J. T. Mathis (2018), Arctic Ocean CO_2 uptake: an improved multiyear estimate of the air–sea CO_2 flux incorporating chlorophyll *a* concentrations, *Biogeosciences*, 15, 1643-1661, doi.org/10.5194/bg-15-1643-2018.

Supplemental Information

Additional data: All of the gridded pCO_2 and ice concentration data from the maps (Figure 1) are plotted together in Figure 1S. These data reveal an overall upward trend of pCO_2 with decreasing ice cover. Interannual differences are not clear, however. Consequently, each cruise data set was averaged to obtain Figure 2. The data after DOR, i.e. the Figure 1S data from 0-15% ice concentration, are the data that are plotted in Figure 3.

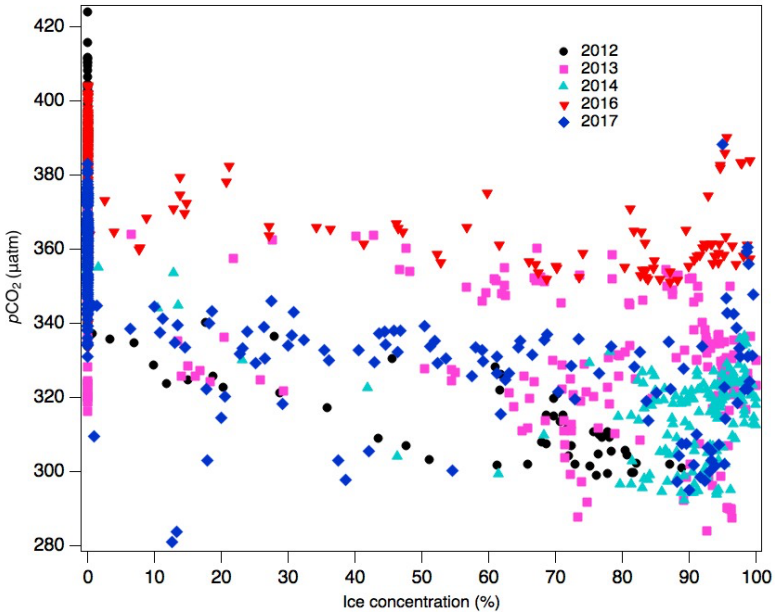

Figure 1S: Gridded pCO_2 and ice concentration data for the area bracketed by 155-130° W, 72-82° N in the Canada Basin (Figure 1).

Mass balance model sensitivity: Model sensitivity to different input variables is illustrated by comparisons with the 2012 model from Figure 3 using 2012 average conditions (black curves in Figure 2S). Model inputs were varied over the range expected based on the inter-annual differences and standard deviations in Table 1 (MLD, wind speed and temperature) and the range of NCP in *Ji et al.* (2019). Results were similar for other years. The 2012 gridded pCO_2 data are included as in Figure 3 to compare the full range of observed variability with the range predicted by the model. Each sensitivity run includes the contribution from heating so that sensitivity model curves and the 2012 model are directly comparable. These results show that much (but not all) of the

variability observed during 2012 can be explained by variability in model input values, discussed in more detail in the manuscript. Sensitivities are shown in Table 1S, calculated from the relative standard deviation of the pCO_2 divided by the relative standard deviation of the variable, i.e.,

S = [(sd pCO_2 mean)/(pCO_2 mean)]/[(sd variable)/[(variable mean)] Equation 1S

where S is the sensitivity in %/%, "sd pCO_2 mean" is the average standard deviation of the model pCO_2 from the 2012 Figure 3 curve (i.e., the deviations of the colored curves from the black curve) and "sd variable" is the standard deviation of the variable over the ranges shown in the legends in Figure 2S. The sensitivities (Table 1S) are small values

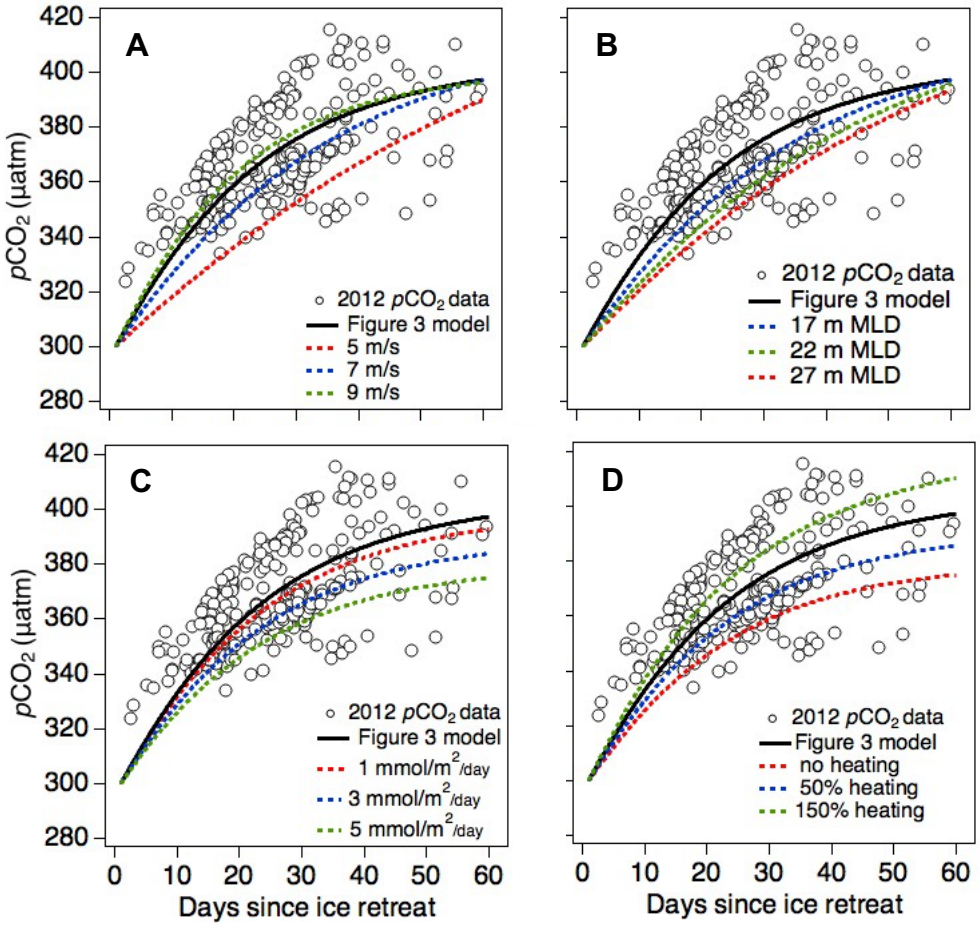

Figure 2S: Sensitivity of the model (see Methods) to different input values for 2012 including wind speed (A) mixed layer depth (B), net community production (NCP)(C) and heating (D). Values were varied over the ranges shown in Table 1. NCP was varied over the range measured by *Ji et al.,* (2019).

because the range of pCO_2 is large relative to the differences in pCO_2, in contrast to the variable (e.g. wind) relative standard deviations which are large (the denominator). The numbers can be compared, however, to provide insight into the potential importance of each variable. To facilitate this comparison, the sensitivities are normalized to the sensitivity due to heating (Table 1S). Results are most sensitive to wind speed, reflecting the non-linear (quadratic) relationship between wind speed and gas transfer velocity (Wanninkhof 2014).

Table 1S: Sensitivity analysis comparisons.

Sensitivity	**%/%**	**relative to heating**
Heating	0.037	1.00
MLD	0.047	1.27
Wind speed	0.090	2.43
NCP	0.025	0.68

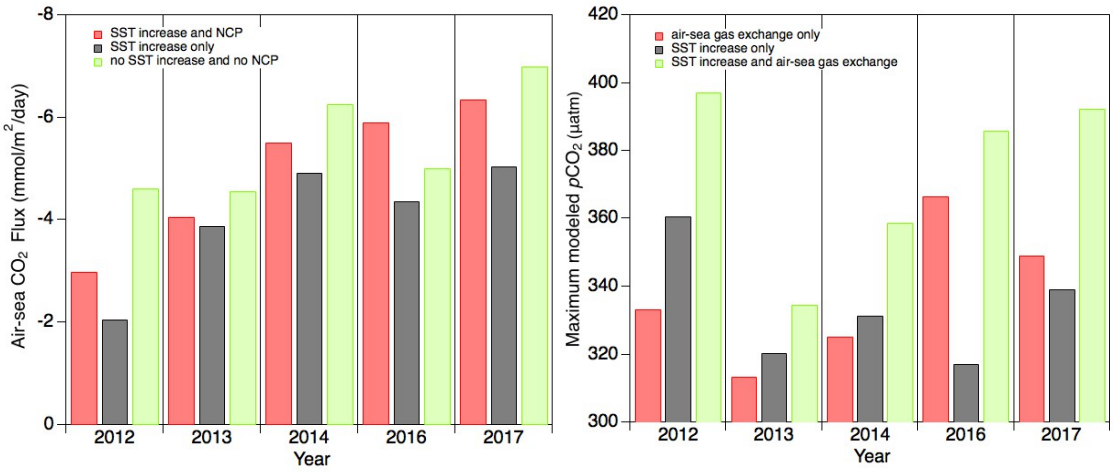

Figure 3S: Modeled air-sea CO_2 fluxes (left) and maximum modeled changes in sea surface pCO_2 (right) for open water. The right figure was derived directly from the model results in Figure 3 using the mean values in Table 2 (no NCP). In the left panel, NCP was set equal to 1.32 mmol m^{-2} day^{-1} (*Ji et al.,* 2019) with and without the SST increase in Table 1.

Effects on air-sea CO_2 fluxes and changes in pCO_2: The model is also used to assess the influence of the SST increase and NCP on the air-sea CO_2 flux (Figure 3S, left panel). These calculations were determined from the model results shown in Figure 3 with SST

warming only or with SST warming and NCP. The fluxes are comparable to other open water air-sea flux values reported for the AO (*Bates et al.*, 2011; *Evans et al.,* 2015). Both SST and NCP can change the net flux of CO_2 by increasing and decreasing the rate of increase of pCO_2, respectively. Fluxes are lowest (within years) when SST is included in the model due to the more rapid increase in pCO_2 towards atmospheric equilibrium. The net air-sea CO_2 flux is lowest in 2012 because the pCO_2 exceeded atmospheric levels and became a source of CO_2 for a short period (Figure 3). For this reason, the increase in SST had the strongest influence in 2012, decreasing the air-sea CO_2 flux by 55% compared to 13-28% during the other years. The model shows that the mean NCP reported in *Ji et al.* (2019) (1.32 mmol m^{-2} d^{-1}) slows the increase in pCO_2, and consequently, increases the flux by 45% in 2012 and from 5-35% during the other years (Figure 3S, left panel). The predicted change in pCO_2 was computed to further illustrate the influence of SST increase on sea surface pCO_2 (Figure 3S, right panel). These results suggest that the relative contributions from the increase in temperature and air-sea gas exchange vary significantly from year to year. For example, contrast the changes in pCO_2 for the larger increase in temperature and shorter maximum DSR in 2012 with the small increase in temperature and long DSR in 2016 (Table 1, Figure 3). Consequently, these results suggest that under current conditions the Canada Basin sink for atmospheric CO_2 will have large inter-annual variability.